iScience, Volume *23*

Supplemental Information

How Repair-or-Dispose Decisions Under Stress Can Initiate Disease Progression

Andreas Nold, Danylo Batulin, Katharina Birkner, Stefan Bittner, and Tatjana Tchumatchenko

Supplemental Information

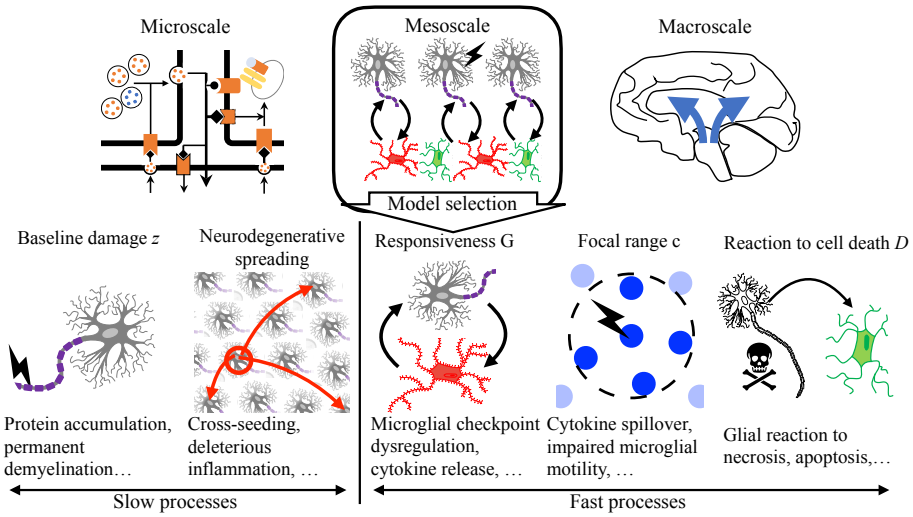

Figure S1: **Five classes of neuron-glia crosstalk are included in a mesoscale model. Related to Figure 2.** We choose a mesoscopic modeling level which generalizes tissue response to a small number of observable factors. It mediates between the microscopic level of cellular and molecular processes (Jolivet et al. 2015) (top left) and the macroscopic level of interacting brain regions (Jucker and Walker, 2013; Weickenmeier et al. 2018) (top right). The model includes the following distinct properties of glia-neuron crosstalk: (i) accumulation of non-repairable baseline damage (z); (ii) slow neuron-to-neuron spreading of baseline damage (S); (iii) glial responsiveness to neuronal damage (G); (iv) focal range of glial reactivity (c); (v) tissue reaction to cell death (D).

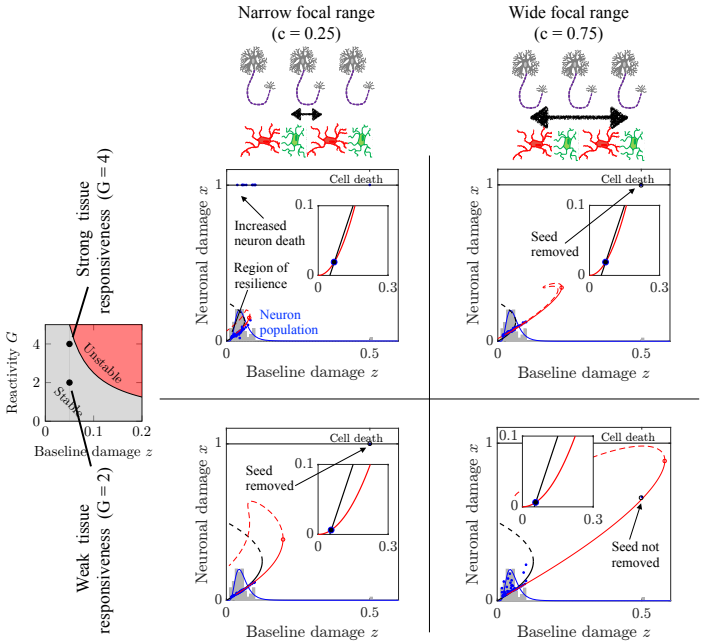

Figure S2: **Functional tissue resilience requires tuning between focal range c and tissue responsiveness G. Related to Figure 3.** Black solid and dashed lines represent stable und unstable steady states in the mean field limit. Red solid and dashed lines represent stable und unstable steady states of one cell for a given (z_n)-distribution. Blue dots represent a population of 200 cells, taken from a log-normal distribution (blue lines). Grey bars represent the histogram of their (z_n)-distribution. Note that some cells are dead (death threshold at unity). For a narrow focal range ($c = 0.25$), cells react more independent of each other (see left column). For a wide focal range ($c = 0.75$), population effects allow for regional compensation of locally elevated stress levels (see top right), but also of rescue of seeds, if the responsiveness G is attenuated (see bottom right). Red and black lines of the insets show mean field damage inducing and damage reducing effects Gx^2 and $x - z$, respectively, as a function of acute damage x.

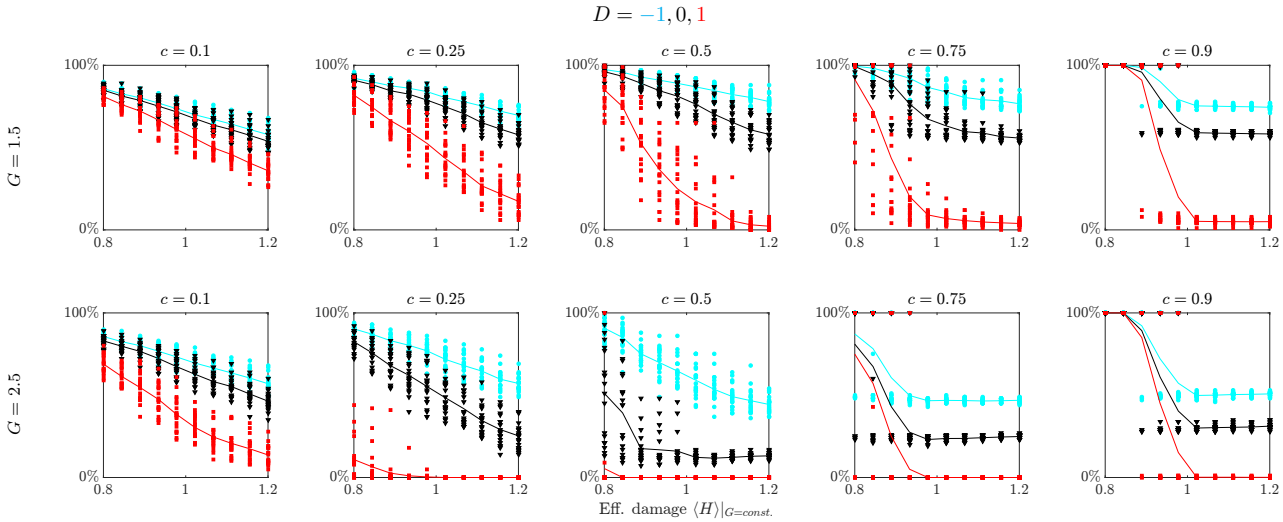

Figure S3: **Critical transition after population increase of baseline damage. Related to Figure 6.** Survival rates after spontaneous cell death for different strengths of responsiveness G for different levels of focal range c, plotted as a function of the effective damage parameter $\langle H \rangle|_{G=const.} = \langle 4Gz \rangle|_{G=const.}$. Simulations with anti-inflammatory, neutral or pro-inflammatory reaction to cell death ($D = -1, 0, 1$) are represented by cyan, black and red lines, respectively. Each symbol represents one distribution of baseline damage levels (z_n), and solid lines connect mean values. Parameters: $N = 100$ in a periodic one-dimensional domain, $t_{\max} = 10$ days, 20 runs per parameter set. Systems with a wide focal range ($c \to 1$) exhibit step-like transitions, for which all cells survive until the critical point is reached, beyond which a steep decrease in survival rates is seen. In contrast, for narrow focal ranges ($c \to 0$), the tissue reacts separately to the stress levels of individual cells, therefore allowing for a gradual decline of survival rates. Protective tissue reactions to cell death ($D = -1$) can act as a barrier for the spread of damage and stabilize cell loss after crossing the critical transition. If protective effects to cell death are attenuated ($D = 0$) or become toxic ($D = 1$), then the death of the first cell sets off a domino-like knock-on effect that can lead to the early death of large parts of the cell assembly. Tissue with intermediate focal range (e.g. $c = 0.5$) is particularly vulnerable to this effect, because local stress by a dying cell fully acts on the neighboring cell, and is not distributed across the tissue. This means that even though the system is stable locally, i.e. small perturbations to the damage levels can be compensated for, it is not stable with respect to the impact of one dying cell, which sets off a propagating lesion.

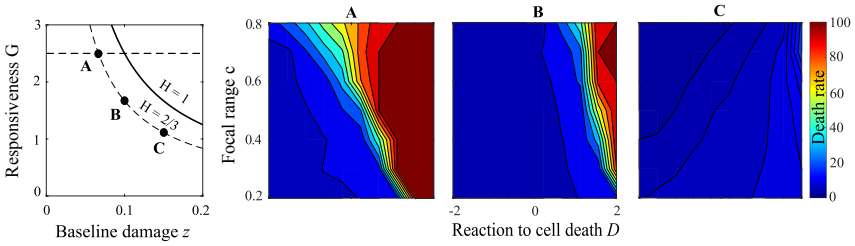

(a) Death rate of a subthreshold stable tissue following an external attack for different baseline damage levels z, as a function of tissue reaction to cell death D and focal range c, for effective responsiveness $\langle H\rangle = 4G\langle z\rangle = 2/3$.

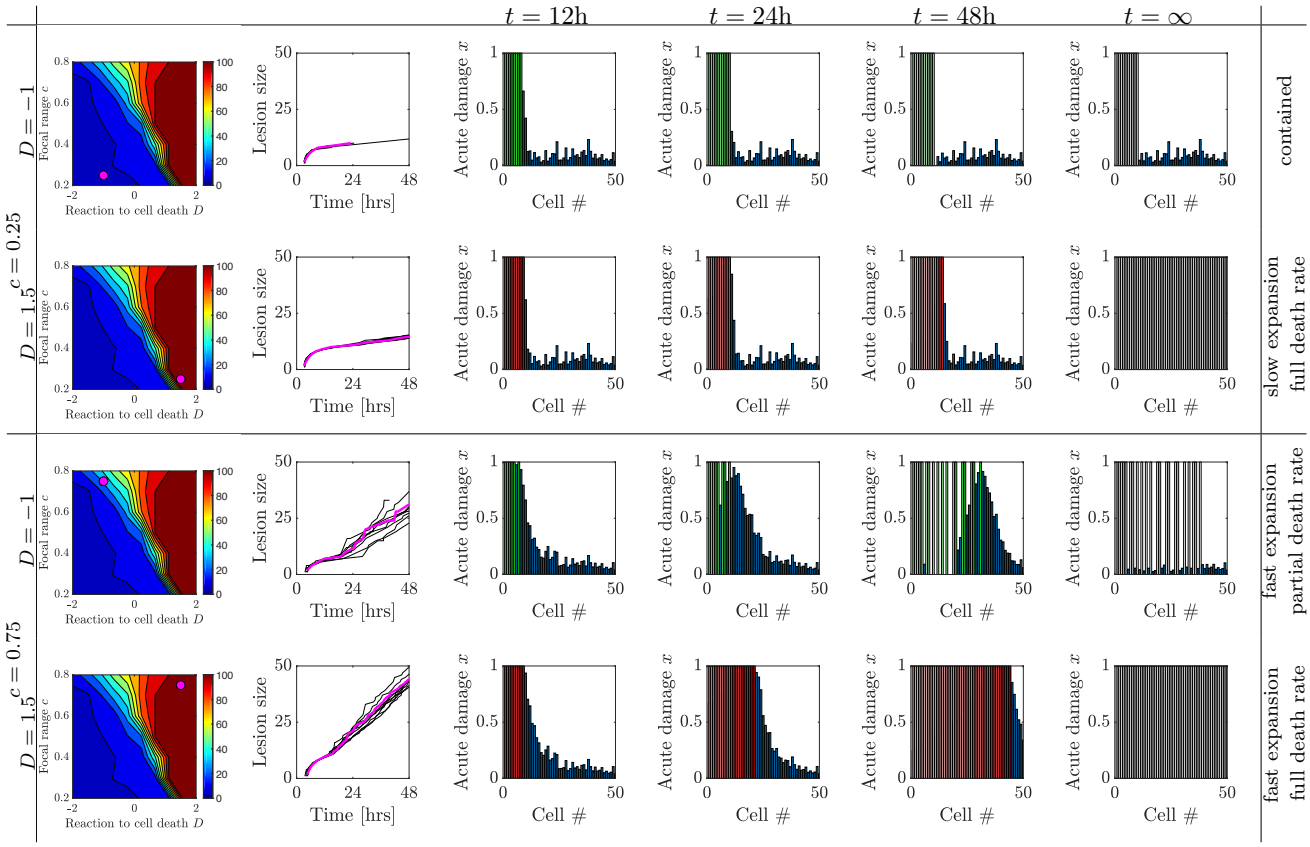

(b) Snapshots of an expanding lesion, initiated by an external injury as in panel **A** of (a) ($G = 2.5$, $\langle H\rangle = 2/3$), for different levels of focal range c and tissue reaction to cell death D. Magenta circles in the plots of the first column depict the chosen parameter set. The colorscale in the first column represents the death rate, as in (a). The second column depicts lesion front paths for 10 (z_n)-distributions. The snapshot panels ($t = 12\text{h}, 24\text{h}, \ldots$) show acute damage values x_n for the path represented by the magenta line. Each bar represents one cell. Blue bars represent amount of damage of alive cells. Bars that reach unity are dead cells. Levels of red and green represents the level of damage-inducing and protective tissue reaction to cell death, respectively.

Figure S4: **Analysis of primed tissue. Related to Figure 6.** Impact of an acute attack on a stable tissue with 100 cells. Here, the stressor function $f_{\text{ext},n} = e^{-t/\tau_{\text{ext}}}[1 - \frac{n}{N_{\text{ext}}}]_+$, is added to the right-hand side of Eq. 3. $\tau_{\text{ext}} = 48$ h and $N_{\text{ext}} = 10$. Acute attacks can initiate wave-like expanding lesions for highly reactive tissues. For a narrow focal range ($c = 0.25$), damage spreads in a domino-like manner from cell to cell. It is contained if tissue reaction to cell-death is protective ($D = -1$), but spreads slowly if tissue reaction to cell death is damage-inducing ($D = 1$). For a wide focal range ($c = 0.75$), a large enough part of the cell population needs to be sufficiently damaged to activate the toxic feedback loop. In this case, the lesion spreads quickly, leading to partial and complete cell death for protective and inflammatory tissue reactions D, respectively.

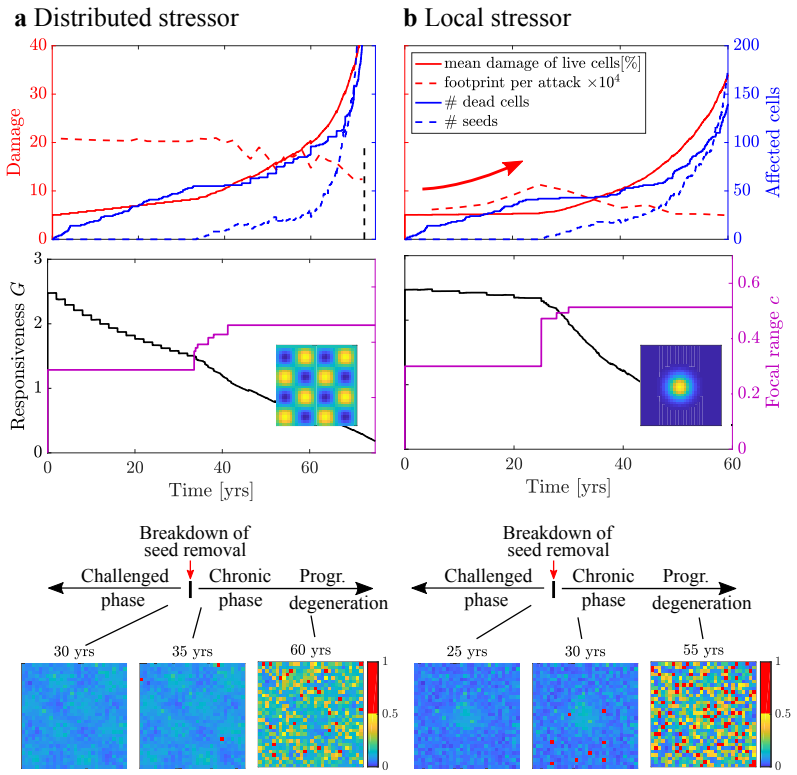

Figure S5: **Long-term stress exposure. Related to Figure 8. Left:** Frequent, weak distributed stressor across the tissue. Gradual adaptation of reactivity G to higher mean damage levels leads to a breakdown of seed removal. **Right:** Repeated, stronger stressor at the center of the domain. Repeated local attacks require an adaptation of the focal range c to maintain short-term stability, leading to a breakdown of seed removal. Prior to this breakdown, the footprint of each perturbation increases (see red arrows). In both scenarios, after the breakdown of seed removal, cell death is first offset because seeds are maintained in the tissue which leads to increasing damage levels. Eventually, cell death rates increase too. Bottom: Baseline damage levels z prior to, immediately after, and long after breakdown of seed removal. Seeds are shown in red. The insets of the graphs of the second row depict the imposed stress pattern. Here, $\tau_\infty = 50$yrs. For model computations without adaptation of G and c, see Figure S6. The following randomly induced stressors were induced: (A) Seeds are induced independently with frequency $\nu = 1/(10\tau_\infty)$. (B) Subthreshold stressors $f_{\text{ext},n}(t) = s(\mathbf{r}_n)\sum_k h(t-t_k)$ are added to the acute cell state are induced at times t_k at rate 1/(2yrs) and 1/(5yrs). Localized subthreshold stressors are modeled with $s(\mathbf{r}_n) = e^{-|\mathbf{r}_n-\mathbf{r}_c|^2/(2\sigma^2)}$ and $\mathbf{r}_c = (n/2, n/2)$. Distributed subthreshold stressors in Figure S5a are modeled with $s(\mathbf{r}_n) = (1+\sin(4\pi(\mathbf{r}_n)_1/n)\sin(4\pi(\mathbf{r}_n)_2/n))/2$. The temporal evolution is $h(t) = \tilde{A}\Theta(t)(1+\tanh((12\text{h}-t)/4\text{h}))/2$ with heaviside function $\Theta(t)$ and $\tilde{A} = 0.1$. After equilibration after each subthreshold stressor at times t_k, baseline damage in increased by $\Delta z = A\int_{t_k}^{\infty}\left(x_n - x_n^{eq}\right)dt$, where x_n^{eq} is the equilibrium state before induction of the subthreshold stressor. $A = 1/500$ and $1/200$ for distributed and local stressors, respectively. After each subthreshold stressor, the parameters c and G were adapted such that: $4G\langle z\rangle < H = 0.5$. The focal range was adapted such that the maximal eigenvalue λ of Eq. (2) remains $\lambda < -0.1/\tau$.

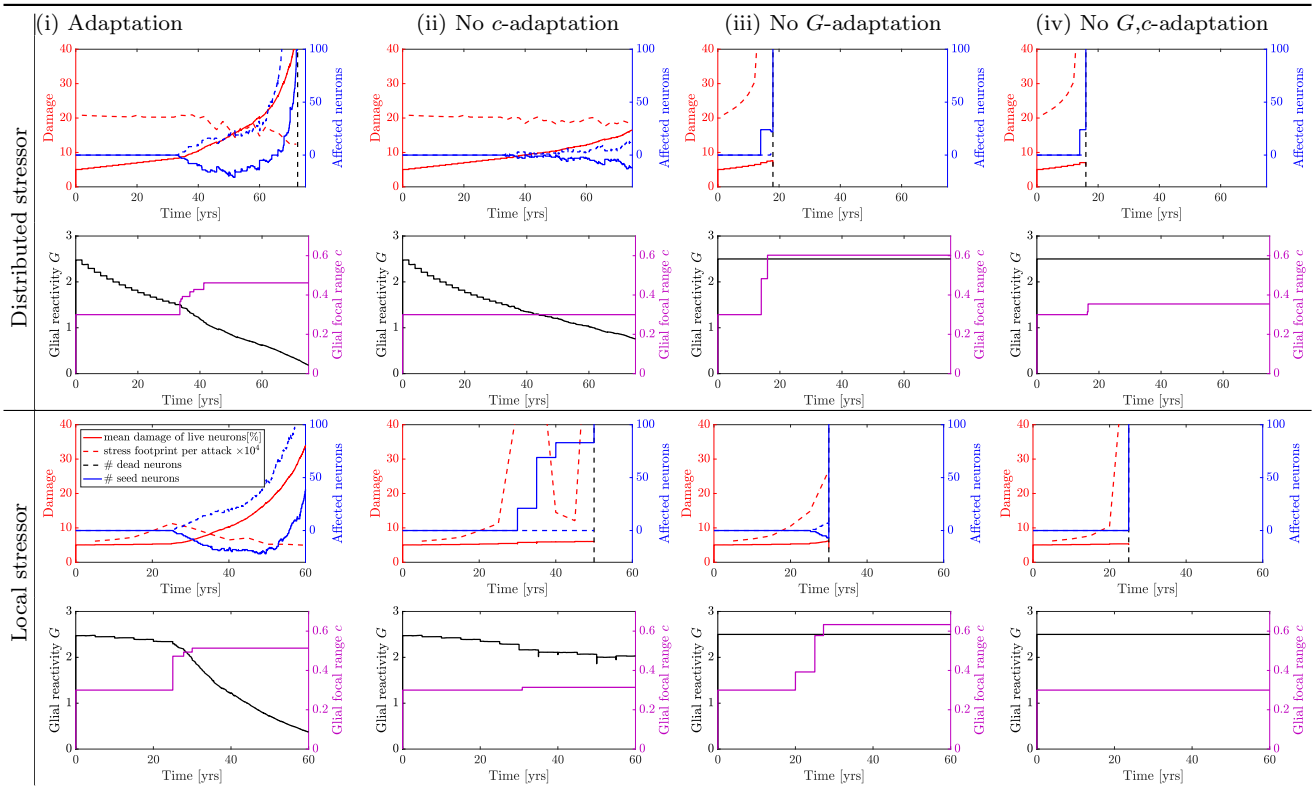

Figure S6: **Lack of adaptation leads to early catastrophic cell loss. Related to Figure 8.** Effect of adaptation of responsiveness G and focal range c for distributed and local stressors as in Figure S5. The first column depicts the results as in Figure S5 of the main manuscript. In the subsequent columns, we deactivate adaptation of c (ii), adaptation of G (iii), and both G and c (iv). In all cases, c is not allowed to adapt beyond 0.6. The black dashed line represents the time point of catastrophic cell loss of more than 100 cells (11%). It is seen how no adaptation leads to early catastrophic cell loss. The distributed stressor model is stabilized by G-adaptation, and the local stressor model is stabilized by both G and c adaptation.

Transparent Methods

S1. Details of numerical simulations

If not stated otherwise, baseline neuronal damage levels z_n are independently drawn from a log-normal distribution, where mean and standard deviation are given in the figure captions. The spatial coupling term $s(r)$ in Eq. 3 is normalized such that in the given domain, $\sum_m s\left(|\mathbf{r}_n - \mathbf{r}_m|\right) = 1$. Simulations at the fast time scale were computed with step $\Delta t = 0.005$hrs, with a first-order Euler forward method. Simulations were implemented on Matlab2018a.

S2. Mean field and steady state solutions

The mean field limit of Eq. 3 is defined by $x_n = x, g_n = g, z_n = z$ constant for all n. In this case, if the cells are alive ($x < 1$), then $g = Gx^2$, and the acute damage x solves $\tau \frac{\mathrm{d}x}{\mathrm{d}t} = -(x - z) + Gx^2$, with steady states given by $x_\pm = (1 \pm \sqrt{1 - 4Gz})/(2G)$ if $z < z_{\mathrm{crit}} = 1/(4G)$. Here, x_+ and x_- are the unstable and stable solutions, depicted in Figure 3. The critical point, beyond which no stationary solution exists, is given by z_{crit}, see also Figure S2.

S3. Focal range c

The interplay between responsiveness G and focal range c determines the tissue reaction to cell damage. It therefore determines whether seed removal is functional or not. In Figure S2, the population effect of four configurations of G and c is shown as an example. In the following, we study the behavior of Eq. 3 of the main manuscript in the limit of very narrow and very wide focal ranges.

If the focal range is very narrow, $c \to 0$, then $\sum_m s(|\mathbf{r}_n - \mathbf{r}_m|) g_m \to g_n$, and we obtain independent ordinary differential equations for all n:

$$\tau \frac{\mathrm{d}x_n}{\mathrm{d}t} = -(x_n - z_n) + g_n. \tag{S1}$$

The results of the mean field section then hold individually for each cell. One side-effect of an increased focal range is that single cells can be maintained, even though their baseline damage z_n exceeds the critical value z_{crit} (see Figures 5 and S2).

If the focal range is very wide, $c \to 1$, we map the discrete values of n onto the spatial variable $\eta = \Delta \cdot n$ with $\Delta = -\log c$. As $c \to 1$, Δ decreases to zero, allowing us to define state variables as functions of η: $x(\eta), g(\eta), z(\eta)$. In the one-dimensional case, d_n in Eq. 3 becomes

$$\begin{aligned} \frac{1-c}{1+c} \sum_{m=-\infty}^{\infty} c^{|n-m|} g_m \quad &= \tfrac{1-c}{1+c} \textstyle\sum_{m=-\infty}^{\infty} e^{-\Delta|n-m|} g_m \\ &\xrightarrow{c\to 1} \tfrac{\Delta}{2} \textstyle\sum_{m=-\infty}^{\infty} e^{-\Delta|n-m|} g_m \\ &\xrightarrow{\Delta\to 0} \tfrac{1}{2} \textstyle\int_{-\infty}^{\infty} e^{-|\eta-\eta'|} g(\eta') \mathrm{d}\eta', \end{aligned}$$

where we used that $\frac{1-c}{1+c} \to \frac{\Delta}{2} + O(c-1)^3$ as $c \to 1$. Eq. 3 then becomes an integral equation

$$\tau \frac{\partial x}{\partial t} = -(x - z) + \frac{1}{2} \int_{-\infty}^{\infty} e^{-|\eta-\eta'|} g(\eta') \mathrm{d}\eta'. \tag{S2}$$

Therefore, for highly imprecise reactivities the characteristic length scale is Δ and the influence of one cell on another decays exponentially on that length scale. This can be observed in the snapshots of Figure S4.

Critical transitions. High levels of baseline damage z can destabilize the tissue. This can happen in two ways: First, a sudden large increase of $\langle z \rangle$ can lead to spontaneous cell death across the tissue (see Figure S3). This has different consequences, depending on the focal range c: Systems with narrow focal ranges allow for gradual cell loss when z increases, but systems with wide focal range c react suddenly and collectively. This population effect has been observed in many other biological and ecological systems, for instance when coral reefs are repaired by 'mobile link organisms' from nearby reefs (Scheffer et al. 2012).

As discussed in the main manuscript, in addition to this classical transition, our model also reveals a metastable 'primed state' for intermediate levels of z (see Figure 6). Under normal conditions, this primed tissue appears to be healthy. However, in the event of strong enough perturbation, the tissue amplifies damage and may initiate a wave-like spreading lesion. In general, anti-inflammatory reactions to cell death (negative D) protect the surrounding tissue against these knock-on effects. If this protection, however, is attenuated, and focal range is wide, then acute attacks can cause widespread damage. Wide focal ranges (high c) and pro-inflammatory reaction to cell death (high D) increases damage. Importantly in this case, the risk of acute short-term damage amplification is more pronounced for a system with intact, high, responsiveness G (see Figure S4 for details).

S4. Seeding parameter S

Equation 1 describes slow damage propagation. We can add a term that represents seeding events that happen at rate ν. After non-dimensionalization, we obtain

$$\frac{\mathrm{d}z_n}{\mathrm{d}t'} = \frac{1}{\nu\tau_\infty} \sum_{m\in\mathcal{C}_n} [z_m - \theta]_+ + z_{\text{cliff}} \sum_k \delta\left(t' - t'_{k,n}\right), \tag{S3}$$

with dimensionless timescale $t' = t\nu$, and where the seeding events $t'_{k,n}$ take place at a rate of one (with respect to the new timescale t'). The early, linear damage propagation is then described by the dimensionless parameter

$$S = \frac{M}{\nu\tau_\infty}. \tag{S4}$$

S represents the balance of the spreading strength M, given by the number of elements in $\mathcal{C}_n$ and speed $1/\tau_\infty$, to the rate of independent self-induced seeding events ν.

Supplemental References

Jolivet, R., Coggan, J.S., Allaman, I., Magistretti, P.J., 2015. Multi-timescale modeling of activity-dependent metabolic coupling in the neuron-glia-vasculature ensemble. PLoS Comput Biol 11, e1004036.

Jucker, M., Walker, L.C., 2013. Self-propagation of pathogenic protein aggregates in neurodegenerative diseases. Nature 501, 45.

Scheffer, M., Carpenter, S.R., Lenton, T.M., Bascompte, J., Brock, W., Dakos, V., van de Koppel, J., van de Leemput, I.A., Levin, S.A., van Nes, E.H., et al., 2012. Anticipating critical transitions. Science 338, 344–348.